Global analysis of scintillation variance: Indication of gravity wave breaking in the polar winter upper stratosphere

V. F. Sofieva,[1] E. Kyrölä,[1] S. Hassinen,[1] L. Backman,[1] J. Tamminen,[1] A. Seppälä,[1] L. Thölix,[1] A. S. Gurvich,[2] V. Kan,[2] F. Dalaudier,[3] A. Hauchecorne,[3] J.-L. Bertaux,[3] D. Fussen,[4] F. Vanhellemont,[4] O. Fanton d' Andon,[5] G. Barrot,[5] A. Mangin,[5] M. Guirlet,[5] T. Fehr,[6] P. Snoeij,[7] L. Saavedra,[6] R. Koopman,[6] and R. Fraisse[8]

Received 11 September 2006; revised 4 December 2006; accepted 14 December 2006; published 8 February 2007.

[1] Stellar scintillations observed through the Earth atmosphere are caused by air density irregularities generated mainly by internal gravity waves and turbulence. We present global analysis of scintillation variance in two seasons of year 2003 based on GOMOS/Envisat fast photometer measurements. Scintillation variance can serve as a qualitative indicator of intensity of small-scale processes in the stratosphere. Strong increase of scintillation variance at high latitudes in winter is observed. The maximum of scintillation variance can be associated with the polar night jet. The simplified spectral analysis has shown the transition of scintillation spectra toward small scales with altitude, which is probably related with turbulence appearing as a result of wave breaking. The breaking of gravity waves in the polar night jet seems to start in the upper stratosphere, a predicted, but not confirmed by observations before, feature. Weaker enhancements in tropics are also observed; they might be related to tropical convection. **Citation:** Sofieva, V. F., et al. (2007), Global analysis of scintillation variance: Indication of gravity wave breaking in the polar winter upper stratosphere, *Geophys. Res. Lett.*, *34*, L03812, doi:10.1029/2006GL028132.

1. Introduction

[2] Propagation of internal gravity waves (IGW) and their breaking into turbulence are of fundamental importance for mean circulation and mixing of the middle atmosphere [*Fritts and Alexander*, 2003; *Gavrilov and Fukao*, 2004]. The global general circulation models still exhibit significant deviations from observations, which are assumed to be due to inadequate parameterization of gravity waves drag [*Austin et al.*, 2003; *Hamilton et al.*, 1999]. Using satellite measurements of stellar scintillation is a new approach that allows studying small-scale processes in the stratosphere. IGW and turbulence create fluctuations of air refractivity (which are proportional to fluctuations of air density) that are observable by remote sensing instruments. When a star is observed on board a satellite, the stellar flux I passed through the atmosphere exhibits scintillation. Due to almost exponential decrease of air density with altitude, the irregularities close to ray perigee produce the main contribution to the observed scintillations.

[3] Analyses of previous stellar scintillation measurements on board the MIR station have allowed determination of statistical and spectral properties of scintillation [*Gurvich et al.*, 2001a, 2001b], and retrieval of parameters of IGW and turbulence spectra [*Gurvich and Kan*, 2003a, 2003b]. An important advantage of using scintillation measurements is that they allow probing small-scale air density irregularities (from few kilometers down to fractions of a meter (MIR)/few meters (GOMOS)) and provide information about IGW and turbulence activity at altitudes $\sim$30–50 km, where other measurements of air density fluctuations at these scales are very scarce. However, the man-controlled photometer on board MIR has provided only a small number of observations. In addition, stellar occultations at latitudes outside the band $\pm 60^\circ$ were not possible with the MIR orbit.

[4] The scintillation measurements became available with global coverage since the launch of the Envisat satellite in March 2002. The GOMOS (Global Ozone Monitoring by Occultation of Stars) instrument on board Envisat is equipped with two fast photometers operating at blue (470–520 nm) and red (650–700 nm) wavelengths with a sampling frequency of 1 kHz http://envisat.esa.int/instruments/gomos). The photometers record stellar flux continuously as a star sets behind the Earth limb.

[5] The main parameter attributed to scintillation is the variance β^2 of relative fluctuations of measured flux I:

$$\beta^2 = \left\langle \frac{(I - \langle I \rangle)^2}{\langle I \rangle^2} \right\rangle. \quad (1)$$

Angular brackets in (1) denote the sample mean. The quantity β is usually called (also in this paper) the scintillation index. The scintillation variance can serve as an indicator of strength of the small-scale processes in the atmosphere.

[6] In this paper, we consider global distribution of the scintillation variance in two seasons of year 2003 with the

[1]Finnish Meteorological Institute, Helsinki, Finland.
[2]A. M. Oboukhov Institute of Atmospheric Physics, Moscow, Russia.
[3]Service d'Aeronomie du CNRS, Verrieres-le-Buisson, France.
[4]Institut d'Aeronomie Spatiale de Belgique, Brussels, Belgium.
[5]ACRI-ST, Sophia-Antipolis, France.
[6]European Space Research Institute, European Space Agency, Frascati, Italy.
[7]European Space Research and Technology Centre, European Space Agency, Noordwijk, Netherlands.
[8]EADS-Astrium, Toulouse, France.

0094-8276/07/2006GL028132

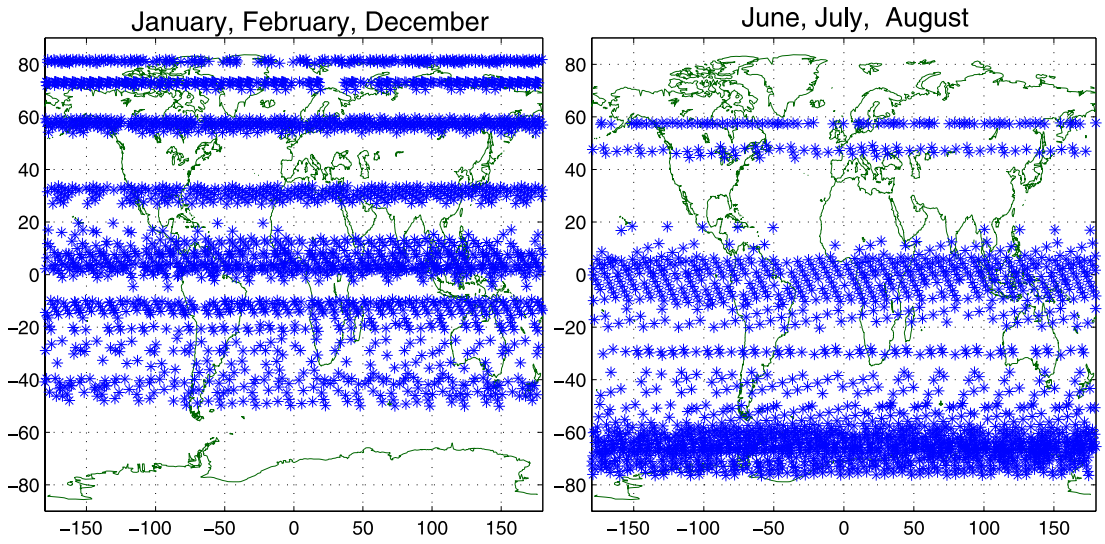

Figure 1. Location of occultations used for analysis.

aim of finding indications of IGW and turbulence activity in the stratosphere.

2. Data Selection and Processing

[7] Locations of 4510 occultations of 30 brightest stars in two seasons of 2003 selected for analysis are shown in Figure 1. We consider dark limb occultations only (scattered solar light prevents star observations during day time), therefore the summer polar atmosphere is not covered. The scintillation variances of blue and red photometer signals are practically identical at altitudes above 30 km. Therefore, we present results only for the red photometer measurements, as they are less affected by absorption and scattering in the atmosphere.

[8] Examples of scintillation measurements by the red photometer are shown in Figure 2, top. The scintillation variance, as well as the maximal altitude, at which scintillation become observable over the noise background, can be very different depending on location and season. This is illustrated in Figure 2, where signals from the red photometer in two occultations of Sirius carried out in different geographic locations and seasons are shown. In this example, the difference in scintillation index (Figure 2, bottom) reaches an order of magnitude at altitudes 50–55 km. The theory [*Tatarskii*, 1971] predicts growth of average scintillation index with decreasing altitude nearly proportional to air density until saturation, which occurs usually at altitudes 25–30 km for GOMOS. This saturation corresponds to the regime of strong scintillation. In our analysis, we concentrate on altitude range above 30 km. At lower altitudes, the saturation complicates significantly the ability to obtain information about air density irregularities from scintillation measurements [*Gurvich et al.*, 2006].

[9] For each occultation, the photometer signal was divided into sections corresponding to a vertical range of ~3 km for ray perigee altitudes. The scintillation variance for each section can be computed using the standard formula for sample variance or as $\sigma_0^2 = \int W(f)df$, where $W(f)$ is the power spectrum of relative fluctuations of photometer signal. The frequency spectrum $W(f)$ is related with the spatial wave-number spectrum $V(k)$ via the relation $W(f)\,df = V(k)\,dk$, where $k = f/u$, u is the ray perigee vertical velocity). Although we selected only occultations of very bright stars (magnitude < 1.6) for the analysis, the signal-to-noise ratio (the "signal" means scintillations) depends on the stellar brightness, especially at higher altitudes (above ~45 km). Therefore, the estimated instrumental noise variance is subtracted from the scintillation variance values:

$$\beta^2 = \sigma_0^2 - \frac{\sigma_{noise}^2}{\langle I \rangle^2}. \tag{2}$$

[10] Here noise of photometers (shown in Figure 2, bottom) consists of photon noise, $\sigma_{phot}^2 \approx \langle I \rangle$, and dark current noise of CCD, σ_{dark}^2: $\sigma_{noise}^2 = \sigma_{phot}^2 + \sigma_{dark}^2$. For the selected occultations, instrumental noise $\sigma_{noise}/\langle I \rangle$ does not exceed 1%. Thus the profile of scintillation variance corresponding to each occultation is obtained.

[11] In case of the GOMOS photometer, the contributions to scintillation variance caused by gravity waves and by turbulence depend on altitude and can be of similar magnitude [*Gurvich et al.*, 2005]. The spectral model that describes scintillation spectra is discussed in detail in [*Gurvich and Kan*, 2003a; *Gurvich and Chunchuzov*, 2005]. It assumes that the scintillation spectrum is the sum of two components, anisotropic (corresponding to IGW) and isotropic (corresponding to turbulence). Observational data [*Gurvich and Kan*, 2003a; *Gurvich and Chunchuzov*, 2005] show that GOMOS photometers suit well for study of the anisotropic component. The sampling rate of GOMOS photometers does not allow observing the isotropy spectrum at high wave numbers (the upper limit is defined by the Fresnel scale): at wave numbers $k < k_N$ (k_N is the wave number corresponding to the Nyquist frequency) available from GOMOS measurements, the isotropy spectrum is practically constant (Figure 3). In order to separate

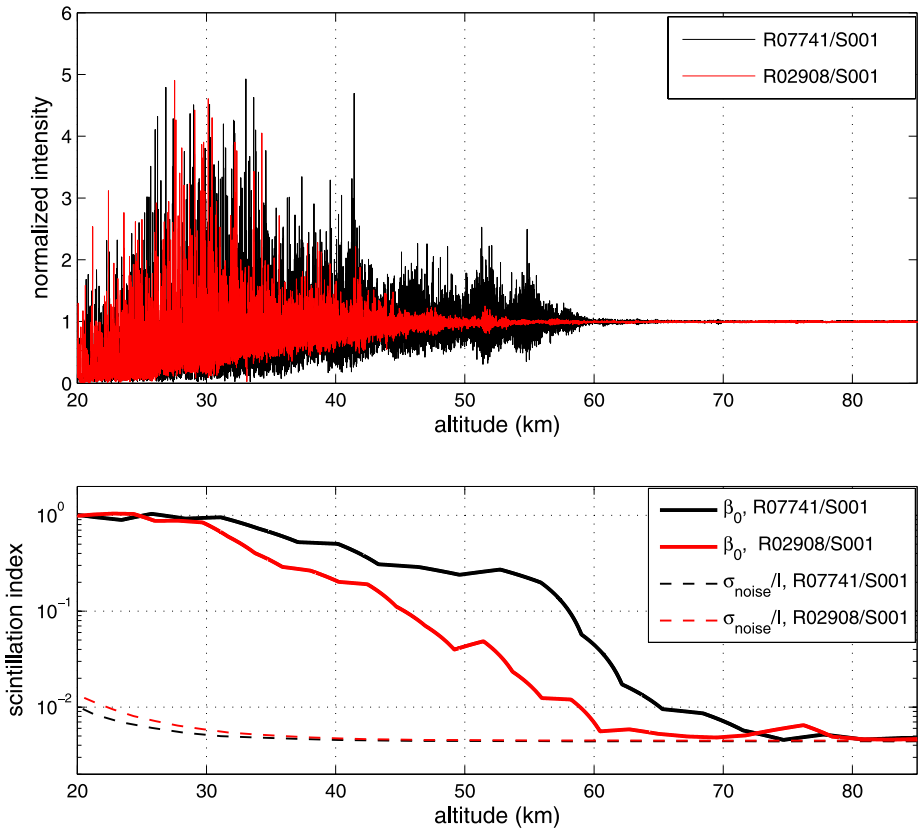

Figure 2. (top) Photometer signals by the GOMOS red photometers in occultations R07741/S001 (62°S, 7°E, 23 August 2003 23:51 UTC) and R02908/S001 (37° S, 106°W, 20 September 2002 07:01 UTC). (bottom) Scintillation index (β) for these two occultations.

wave and turbulent contributions to the scintillation variance, we calculated the high-frequency variance:

$$\beta^2_{high} = \int_{k_{high}}^{k_N} V(k)dk, \tag{3}$$

where the wave number k_{high} is chosen equal to k_{high} = 1/8 cyc/m (Figure 3). The corresponding vertical scale l_{high} = 8 m is smaller than the typical inner scale l_W = $1/\kappa_W$ of the IGW spectrum [*Gurvich and Kan*, 2003a; *Gurvich and Chunchuzov*, 2005]. The shape of the isotropy spectrum allows removal of the turbulent contribution from the scintillation variance and computing low-frequency variance β^2_{low} that contains mainly IGW contribution (see Figure 3 for illustration):

$$\beta^2_{low} = \beta^2 - \beta^2_{high}\frac{k_N}{k_N - k_{high}}. \tag{4}$$

[12] To estimate the variance corresponding to turbulent component, β^2_{iso}, we approximate the isotropic spectrum by the equivalent rectangle with area equal to β^2_{iso} (Figure 3, right). It is bounded at high wave numbers by k_{Fr}, the wave number corresponding to the Fresnel scale ($Fr = \sqrt{\lambda L}$, λ is wavelength and L is the distance from ray perigee to the satellite, Fr ~1.4 m for the GOMOS red photometer). Then the scintillation variance corresponding to the turbulent component β^2_{iso} can be computed as

$$\beta^2_{iso} = \beta^2_{high}\frac{k_{Fr}}{k_N - k_{high}}. \tag{5}$$

[13] Only oblique (off orbital plane) occultations were selected for this analysis, in order to better separate wave and turbulent contributions to scintillation variance [*Gurvich and Kan*, 2003a]. Since the chromatic smoothing over the finite wavelength band of optical filters reduces slightly the spectral density of isotropic scintillations at lowermost altitudes, we applied a normalization that takes into account the chromatic distortion.

[14] Assuming that the scintillations result from air density irregularities generated by a random ensemble of IGW with one-dimensional vertical spectrum $V_T(k)$ = $A\omega^4_{BV}\, g^{-2}\, k^{-3}$ (the saturated gravity waves model [e.g., *Fritts and Alexander*, 2003]), the scintillation variance β^2_{IGW} can be estimated as

$$\beta^2_{IGW} \approx 2\pi R_E A L^2 \kappa_W \omega^4_{BV} g^{-2} \nu^2 q^2, \tag{6}$$

where R_E is the Earth radius, ω_{BV} is the Brunt-Väisälä frequency, g is acceleration of gravity ν is refractivity and q is refractive dilution. The formula (6) is obtained using approximation of geometric optics and phase screen model of the atmosphere [*Gurvich and Brekhovskikh*,

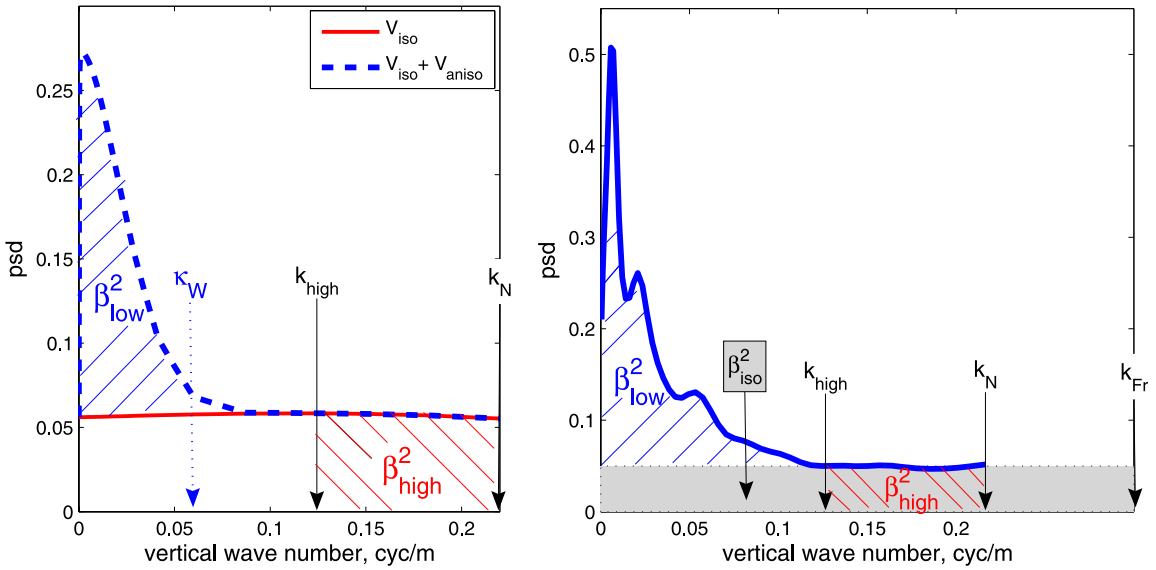

Figure 3. (left) Scintillation spectrum for two-component model of air density irregularities [*Gurvich and Kan*, 2003a; *Gurvich and Chunchuzov*, 2005] consists of two components: V_{aniso}, which is generated by anisotropic irregularities (corresponding to IGW), and V_{iso}, which is generated by isotropic irregularities (mainly turbulence). Shaded areas indicate the high-frequency and low-frequency variances. The area under the curve V_{iso} corresponds to the correction term $\beta^2_{high}\frac{k_N}{k_N-k_{high}}$ in (4). (right) Scintillation spectrum for the occultation R02908/S001 at 40 km. Shaded areas indicate β^2_{high}, β^2_{low} and β^2_{iso} given by (3), (4) and (5), respectively.

2001]. The estimate β^2_{IGW} corresponds to the experimental variance β^2_{low}. As follows from (6), β^2_{low} can serve as a qualitative indicator of gravity waves activity: it depends on combination of parameters defining IGW spectrum.

[15] The scintillation variance corresponding to the Kolmogorov's model of locally isotropic turbulence is proportional to the structure characteristic C_n^2 of refractivity fluctuations: $\beta^2_{iso} \propto C_n^2 = \nu^2 C^2$ (here C^2 is the structure characteristic of relative refractivity fluctuations). Therefore, variations of experimental scintillation index β_{iso} normalized on refractivity are caused mainly by variations in C^2 .

3. Results and Discussion

[16] Figures 4a and 4b (color, logarithmic scale) show the zonal mean scintillation index β in two seasons of year 2003. For data averaging, we calculated zonal mean in latitudinal bins distributed in accordance with available data (Figure 1). The width of latitudinal bins is mainly ~10°, but it ranges from 5° to 30°. The maps are almost symmetric for these two seasons. The scintillation index rapidly grows with decreasing altitude. The saturation ($\beta \approx 1$) is achieved at ~30 km in winter mid- and high-latitude atmosphere and at ~25 km in equatorial regions. The enhanced scintillation index is clearly observed at mid- and high latitudes in winter and in tropical summer atmosphere. The overlaid contours in Figures 4a and 4b show the logarithm of the model scintillation index β_{IGW} (6) computed using ECMWF temperature and air density analysis data at the occultation locations, the mean experimental value $A = 0.1$ and the inner scale of the scintillation spectra $l_W = 15$ m. Although (6) explains well the mean dependence on altitude, the latitudinal variations in air density and Brunt-Väisälä frequency do not explain the observed latitudinal dependence of the scintillation index, as seen in Figures 4a and 4b.

[17] Figures 4c and 4d (color, linear scale) show the scintillation index β_{low} divided by refractivity ν (with scaling factor 10^{-5}). This normalization removes the main altitude dependence of the scintillation index and the variations caused by differences in air density at different locations (equation (6)). Strong maxima at winter polar and mid-latitude atmosphere and significantly weaker enhancements in the tropical atmosphere are observed. These enhancements in β_{low} are to be related to internal gravity waves. The annual cycle in gravity wave energy at altitudes 30–50 km at high and middle latitudes with maximum in winter and minimum in summer was observed previously in rocket sounding (at ~1 km resolution) [*Hirota*, 1984; *Hamilton*, 1991, *Eckermann et al.*, 1995] and lidar data (resolution ~1km) [*Wilson et al.*, 1991; *Whiteway and Carswell*, 1995]. It has been discussed that the mean atmospheric conditions largely induce the horizontal, vertical and temporal variations of the gravity wave field in the stratosphere and mesosphere through filtering of gravity waves [*Wilson et al.*, 1991; *Fritts and Alexander*, 2003]. We can expect a larger scintillation index in the high-latitude winter stratosphere due to increased Brunt-Väisälä frequency (the overlaid contours in Figure 4c and 4d represent $\omega^2_{BV} \cdot 10^4$ (rad^{2}s^{-2}) computed at the occultation locations using ECMWF temperature data and averaged in the same way as the scintillation index). However, the variations in the thermal structure, as measured by Brunt-Väisälä frequency, cannot explain quantitatively the 3–4 times increased scintillation index at winter high latitudes (compared to other locations) and its latitudinal pattern with the sharp maximum at latitude ~70°. The position of the scintillation index maxima prompts us assuming that the increased scintillation variance might be also related with the dynamical processes close to the edge of polar vortex (see also below). IGW with vertical scales from few meters

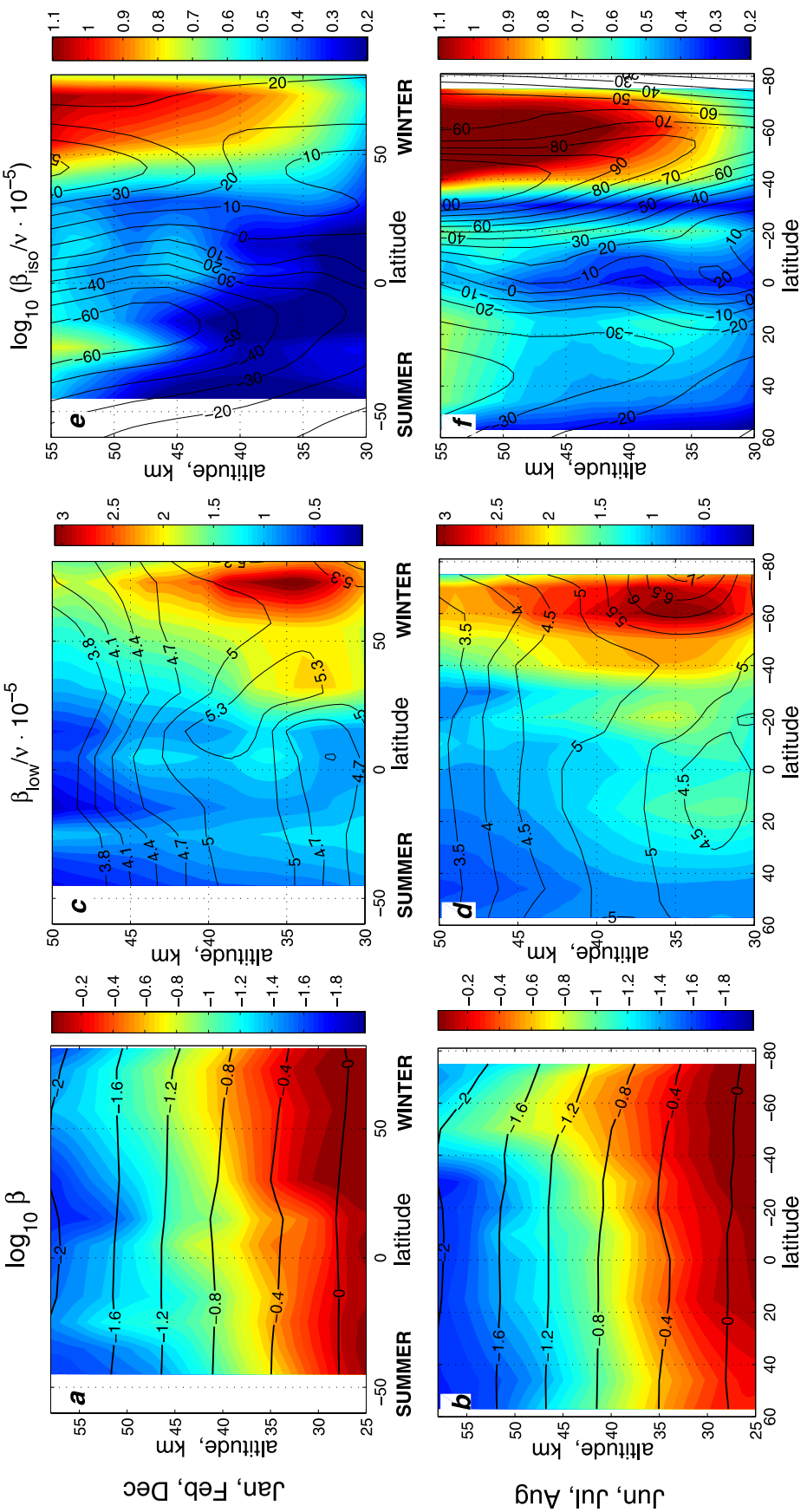

Figure 4. (a, b) Zonal mean scintillation index ($\log_{10}\beta$) (color) and $\log_{10}\beta_{IGW}$ computed using ECMWF temperature and density (black contours). (c, d) β_{low} (color) normalized on ν (color) and $\omega_{BV}{}^2$ (rad^{2}s^{-2}) computed using ECMWF temperature at occultation locations (black contours) (e, f) $\log_{10}(\beta_{iso}/\nu{\cdot}10^{-5})$ (color) and mean zonal wind (m/s) from ECMWF analysis data (black contours). Figures 4a, 4c, and 4e show data for January, February and December, and Figures 4b, 4d, and 4f show data for June, July and August 2003 (note the reverse scale on x-axis).

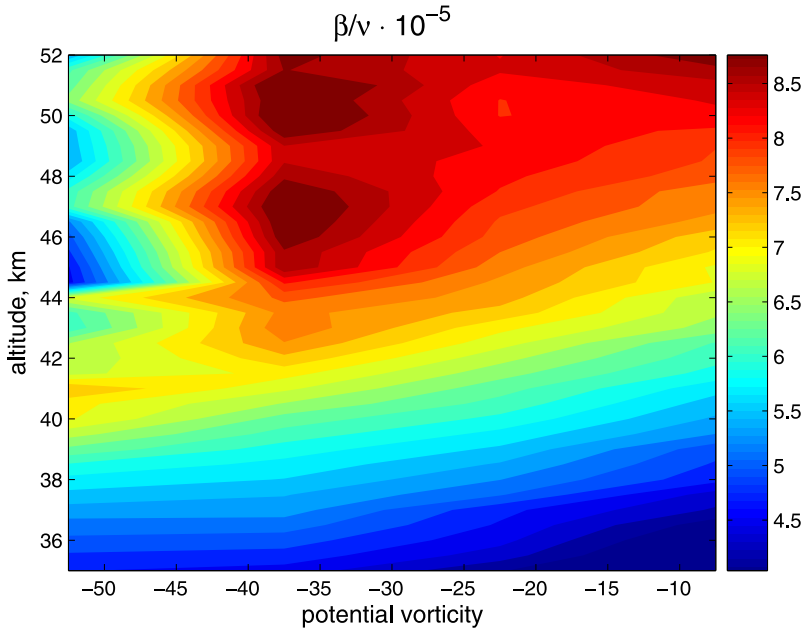

Figure 5. Scintillation index β with normalization on refractivity as a function of potential vorticity, for occultations located at 50–75° S in July and August 2003. The value 36 PVU is often used as a boundary of the polar vortex.

to few kilometers that generate observed scintillations seem to have favorable conditions for propagating in the polar winter atmosphere.

[18] Figures 4e and 4f (color, logarithmic scale) show β_{iso} normalized on refractivity, which corresponds to the turbulent component of the scintillation index. Strong enhancements at high latitudes in winter are observed; they are the extensions of the corresponding IGW maxima in Figures 4c and 4d to higher altitudes. The transition of the scintillation spectra toward smaller scales with altitude allows us to suggest that it is related with breaking of gravity waves and consecutive appearance of turbulence at altitudes above ~45 km. The capability of gravity waves to propagate from tropospheric sources to the stratosphere is largely determined by the interaction with wind. A relatively good correlation of β_{iso} with mean zonal winds calculated from ECMWF analysis data is observed (contours in Figures 4e and 4f). The enhancement of β_{iso} at winter high latitudes is much larger in Southern Hemisphere. This is probably related to larger wind speed in Antarctic polar jet. Several previous observational studies [*Duck et al.*, 1998, 2001; *Jiang and Wu*, 2001] found increased IGW activity associated with polar vortex jet and pointed out that the gravity waves should break in the polar night jet at altitudes close to stratopause, in order to explain the thermal balance in the polar vortex area. The GOMOS observations provide first observational support for this hypothesis.

[19] Intensity of gravity waves and mixing processes are expected to be low in the core of the polar vortex, due to isolation of this part of the atmosphere and strong critical level filtering of gravity waves. Conversely, high activity of gravity waves observed in scintillation data might be associated with the polar night jet, where less critical level filtering is encountered. Figure 5, which shows distribution of scintillation index as a function of potential vorticity, for occultations located 50–75° S in July and August 2003, illustrates this: scintillation variance has a maximum at ~36–37 PVU (these potential vorticity values are associated usually with the polar vortex edge). The transition of the scintillation spectra toward smaller scales in the regions of high scintillation index (Figure 4) seems to be related with the gravity waves breakdown into turbulence.

[20] There are also enhancements in scintillation index (both in β_{low} and β_{iso}) over tropical regions, which are significantly weaker compared to that in polar regions. They might be associated with enhanced IGW activity above tropical convective clouds as reported in previous studies [*Karoly et al.*, 1996; *Shimizu and Tsuda*, 1997].

4. Summary

[21] The scintillations in stellar occultation experiment, which are influenced by small-scale internal gravity waves and turbulence, are a sensitive tool for studying small-scale processes in the stratosphere. In this paper, we have presented first global distributions of scintillation variance in two seasons of 2003 based on scintillation measurements by GOMOS. Strong increase of scintillation variance at high latitudes in winter and less strong enhancements in tropics are observed, which might be related to the polar night jet and tropical convection, respectively.

[22] The analysis has shown that the enhancements of scintillation variance in winter polar atmosphere are related not only with the variations in thermal structure, but also with critical level filtering for gravity waves. The observations show that the maximum of scintillation variance can be associated with the polar night jet. The simplified spectral analysis has shown the transition of scintillation spectra toward small scales with altitude, which is probably related with the turbulence appearing as a result of wave breaking. The breaking of gravity waves seems to start in the upper stratosphere (above ~40–45 km) in the polar night jet. This was predicted [*Duck et al.*, 2001; *Jiang and Wu*, 2001], but, to our knowledge, has not been confirmed

by observations before. Quantitative analysis of scintillation spectra, as proposed by *Gurvich and Kan* [2003a], *Gurvich and Chunchuzov* [2005], and V. F. Sofieva et al. (Reconstruction of internal gravity wave and turbulence parameters in the stratosphere using GOMOS scintillation measurements, submitted to *Journal of Geophysical Research*, 2006), will refine these findings and allow reconstruction of parameters of IGW and turbulence spectra in the stratosphere in future.

[23] **Acknowledgments.** The work of V. F. Sofieva and A. Seppälä was supported by the Academy of Finland. The work of A. S. Gurvich and V. Kan was supported by the Russian Foundation for Basic Research, grant 06-05-64357. Authors thank Finnish Academy of Science and Letters, Vilho, Yrjö and Kalle Väisälä Foundation for the support.

References

Austin, J., et al. (2003), Uncertainties and assessments of chemistry-climate models of the stratosphere, *Atmos. Chem. Phys.*, *3*, 1–27.

Duck, T. J., J. A. Whiteway, and A. I. Carswell (1998), Lidar observations of gravity wave activity and Arctic stratospheric vortex core warming, *Geophys. Res. Lett.*, *25*(15), 2813–2816.

Duck, T. J., J. A. Whiteway, and A. I. Carswell (2001), The gravity wave–Arctic stratospheric vortex interaction, *J. Atmos. Sci.*, *58*, 3581–3596.

Eckermann, S. D., I. Hirota, and W. K. Hocking (1995), Gravity wave and equatorial wave morphology of the stratosphere derived from long-term rocket soundings, *Q.J.R. Meteorol. Soc.*, *121*, 149–186.

Fritts, D. C., and M. J. Alexander (2003), Gravity wave dynamics and effects in the middle atmosphere, *Rev. Geophys.*, *41*(1), 1003, doi:10.1029/2001RG000106.

Gavrilov, N. M., and S. Fukao (2004), Numerical and the MU radar estimations of gravity wave enhancement and turbulent ozone fluxes near the tropopause, *Ann. Geophys.*, *22*, 3889–3898.

Gurvich, A. S., and V. L. Brekhovskikh (2001), Study of the turbulence and inner waves in the stratosphere based on the observations of stellar scintillations from space: A model of scintillation spectra, *Waves Random Media*, *11*, 163–181.

Gurvich, A., and I. Chunchuzov (2005), Estimates of characteristic scales in the spectrum of internal waves in the stratosphere obtained from space observations of stellar scintillations, *J. Geophys. Res.*, *110*, D03114, doi:10.1029/2004JD005199.

Gurvich, A. S., and V. Kan (2003a), Structure of air density irregularities in the stratosphere from spacecraft observations of stellar scintillation: 1. Three-dimensional spectrum model and recovery of its parameters, *Izv. Russ. Acad. Sci. Atmos. Oceanic Phys.*, Engl. Transl., *39*, 300–310.

Gurvich, A. S., and V. Kan (2003b), Structure of air density irregularities in the stratosphere from spacecraft observations of stellar scintillation: 2. Characteristic scales, structure characteristics, and kinetic energy dissipation, *Izv. Russ. Acad. Sci. Atmos. Oceanic Phys.*, Engl. Transl., *39*, 311–321.

Gurvich, A. S., et al. (2001a), Studying the turbulence and internal waves in the stratosphere from spacecraft observations of stellar scintillation: I. Experimental technique and analysis of the scintillation variance, *Izv. Russ. Acad. Sci. Atmos. Oceanic Phys.*, Engl. Transl., *37*, 436–451.

Gurvich, A. S., V. Kan, S. A. Savchenko, A. I. Pakhomov, and G. I. Padalka (2001b), Studying the turbulence and internal waves in the stratosphere from spacecraft observations of stellar scintillation: II. Probability distributions and scintillation spectra, *Izv. Russ. Acad. Sci. Atmos. Oceanic Phys.*, Engl. Transl., *37*, 452–465.

Gurvich, A. S., F. Dalaudier, and V. F. Sofieva (2005), Study of stratospheric air density irregularities based on two-wavelength observation of stellar scintillation by Global Ozone Monitoring by Occultation of Stars (GOMOS) on Envisat, *J. Geophys. Res.*, *110*, D11110, doi:10.1029/2004JD005536.

Gurvich, A. S., V. V. Vorobjev, and O. V. Fedorova (2006), Evaluation of the spectral parameters of internal waves in the stratosphere based on the observations of strong stellar scintillation from space, *Izv. Russ. Acad. Sci. Atmos. Oceanic Phys.*, Engl. Transl., *42*, 463–472, doi:10.1134/S0001433806040062.

Hamilton, K. (1991), Climatological statistics of stratospheric inertia-gravity waves deduced from historical rocketsonde wind and temperature data, *J. Geophys. Res.*, *96*, 20,831–20,839.

Hamilton, K., R. J. Wilson, and R. S. Hemler (1999), Middle atmosphere simulated with high vertical and horizontal resolution versions of a GCM: Improvements in the cold pole bias and generation of a QBO-like oscillation in the tropics, *J. Atmos. Sci.*, *56*, 3829–3846.

Hirota, I. (1984), Climatology of gravity waves in the middle atmosphere, *J. Atmos. Terr. Phys.*, *46*, 767–773.

Jiang, J. H., and D. L. Wu (2001), UARS MLS observations of gravity waves associated with the arctic winter stratospheric vortex, *Geophys. Res. Lett.*, *28*(3), 527–530.

Karoly, D. J., G. L. Roff, and M. J. Reeder (1996), Gravity wave activity associated with tropical convection detected in TOGA COARE sounding data, *Geophys. Res. Lett.*, *23*(3), 261–264.

Shimizu, A., and T. Tsuda (1997), Characteristics of Kelvin waves and gravity waves observed with radiosondes over Indonesia, *J. Geophys. Res.*, *102*(D22), 26,159–26,172.

Tatarskii, V. I. (1971), *The Effects of the Turbulent Atmosphere on Wave Propagation*, 417 pp., U. S. Dep. of Commer., Springfield, Va.

Whiteway, J. A., and A. I. Carswell (1995), Lidar observations of gravity wave activity in the upper stratosphere over Toronto, *J. Geophys. Res.*, *100*(D7), 14,113–14,124.

Wilson, R., M.-L. Chanin, and A. Hauchecorne (1991), Gravity waves in the middle atmosphere observed by Rayleigh lidar: 2. Climatology, *J. Geophys. Res.*, *96*(D3), 5169–5183.

L. Backman, S. Hassinen, E. Kyrölä, A. Seppälä, V. F. Sofieva, J. Tamminen, and L. Thölix, Finnish Meteorological Institute, Earth Observation, P.O. Box 503, FIN-00101, Helsinki, Finland.

G. Barrot, O. Fanton d' Andon, M. Guirlet, and A. Mangin, ACRI-ST, 260, route du Pin Montard, BP 234, F-06904 Sophia-Antipolis, France.

J.-L. Bertaux, F. Dalaudier, and A. Hauchecorne, Service d'Aeronomie du CNRS, BP 3, F-91371 Verrières-le-Buisson Cedex, France.

T. Fehr, R. Koopman, and L. Saavedra, European Space Research Institute, European Space Agency, I-00044 Frascati, Italy.

R. Fraisse, EADS-Astrium, 31 Avenue des Cosmonautes, F-31402 Toulouse Cedex 4, France.

D. Fussen and F. Vanhellemont, Institut d'Aeronomie Spatiale de Belgique, Avenue Circulaire 3, B-1180 Brussels, Belgium.

A. S. Gurvich and V. Kan, A. M. Oboukhov Institute of Atmospheric Physics, Pyzhevsky 3, Moscow 119017, Russia.

P. Snoeij, European Space Research and Technology Centre, European Space Agency, NL-2200 AG Noordwijk, Netherlands.